Dalton Transactions

ROYAL SOCIETY OF CHEMISTRY

PAPER

View Article Online
View Journal | View Issue

Cite this: *Dalton Trans.*, 2023, **52**, 10574

Robust and efficient transfer hydrogenation of carbonyl compounds catalyzed by *NN*-Mn(I) complexes†

Zheng Wang, *[a,b,c] Ning Ma,[a] Xiaochi Lu,[a] Ming Liu, [b] Tian Liu,[b] Qingbin Liu, *[c] Gregory A. Solan*[b,d] and Wen-Hua Sun *[b]

Received 28th June 2023,
Accepted 10th July 2023

DOI: 10.1039/d3dt02022c

rsc.li/dalton

A series of manganese(I) carbonyl complexes bearing structurally related *NN*- and *NNN*-chelating ligands have been synthesized and assessed as catalysts for transfer hydrogenation (TH). Notably, the *NN*-systems based on *N*-R functionalized 5,6,7,8-tetrahydroquinoline-8-amines, proved the most effective in the manganese-promoted conversion of acetophenone to 1-phenylethanol. In particular, the *N*-isopropyl derivative, **Mn1**, when conducted in combination with *t*-BuONa, was the standout performer mediating not only the reduction of acetophenone but also a range of carbonyl substrates including (hetero)aromatic-, aliphatic- and cycloalkyl-containing ketones and aldehydes with especially high values of TON (up to 17 200; TOF of 3550 h^{-1}). These findings, obtained through a systematic variation of the *N*-R group of the *NN* ligand, are consistent with an outer-sphere mechanism for the hydrogen transfer. As a more general point, this Mn-based catalytic TH protocol offers an attractive and sustainable alternative for producing alcoholic products from carbonyl substrates.

Introduction

The conversion of ketones and aldehydes to their corresponding alcohols constitutes one of the most fundamental reactions and is central to the synthesis of numerous important derivatives such as fragrances, flavors, and fine-chemical intermediates as well as pharmaceuticals.[1] Indeed, a wide range of approaches have been applied over the years to realize this transformation.[1a] Conventionally, stoichiometric amounts of metal hydrides (*e.g.* $NaBH_4$ or $LiAlH_4$) or boranes are employed (Scheme 1a), but these reagents can be problematic on account of their hazardous or toxic properties and moreover can afford large amounts of noxious by-products.[1,2] As an alternative to these stoichiometric approaches, catalytic transfer hydrogenation (TH) protocols offer an attractive and sustainable strategy.[1b,c,3] To this end, precious metal-based catalysts based on Ru,[4] Rh,[5] Ir,[6] or Os[7] have paved the way (Scheme 1b). However, the high cost of some of these complexes and their limited availability of their metal centers poses problems with their long-term application.[3b,8] Therefore, there is a considerable impetus to develop catalysts based on

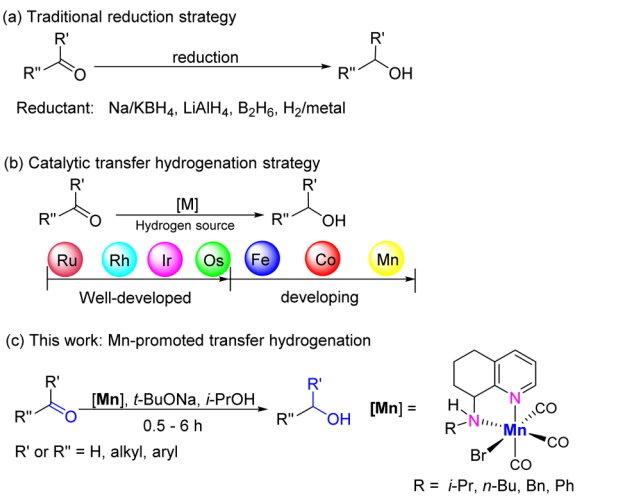

Scheme 1 Strategies for the reduction of ketones or aldehydes to give alcohols.

[a]*College of Science, Hebei Agricultural University, Baoding 071001, China*
[b]*Key Laboratory of Engineering Plastics and Beijing National Laboratory for Molecular Science, Institute of Chemistry, Chinese Academy of Sciences, Beijing 100190, China. E-mail: wangzheng@iccas.ac.cn, whsun@iccas.ac.cn*
[c]*Hebei Key Laboratory of Organic Functional Molecules, College of Chemistry and Material Science, Hebei Normal University, Shijiazhuang 050024, China. E-mail: liuqingb@sina.com*
[d]*Department of Chemistry, University of Leicester, University Road, Leicester LE1 7RH, UK. E-mail: gas8@leicester.ac.uk*

†Electronic supplementary information (ESI) available: Detailed experimental procedures, spectra (NMR), Fig. S1–S53, Tables S1–S6 and X-ray crystallographic data. CCDC 2248092 ([**L1**H]Br) and 2248093 (**Mn1**). For ESI and crystallographic data in CIF or other electronic format see DOI: https://doi.org/10.1039/d3dt02022c

inexpensive and earth-abundant 3d transition metals in combination with robust and synthetically accessible ligand frameworks.[9] As a consequence, a great deal of reports have emerged on the development of iron-[10] and cobalt-[11] based catalysts for TH (Scheme 1b), whereas the use of manganese, the third most abundant metal in the Earth's crust, is rather more limited. Indeed, manganese has traditionally been considered as a metal for promoting oxidation reactions.[12]

Nonetheless, the last six years or so have seen some key advances in Mn-catalyzed TH, particularly with regard to the conversion of ketones to secondary alcohols.[13–15] In 2017, Beller first showed that dipicolylamine-manganese *NNN*-pincer complexes can promote the reduction of ketones using isopropanol as the hydrogen source.[13a] Later, Sortais's group reported the use of Mn(I) complexes bearing bidentate 2-picolylamine ligands[13b] that could facilitate turnover frequencies (TOF) as high as 3600 h^{-1}. Since then, much attention has been dedicated to developing simple air-stable bidentate ligand systems that can facilitate the TH process.[13c–i] However, most of these *NN*-chelated Mn(I)-complexes, including aminotriazole,[13c] benzimidazole[13d] or bipyridine ligands,[13e,f] require high catalyst loading (0.2–3.0 mol%) to achieve good conversions.[13c–g] Elsewhere, Pidko demonstrated that the replacement of one N-donor unit in the *NN*-ligand by an N-heterocyclic carbene resulted in a significant improvement in the Mn-catalyzed TH of ketones. Indeed, an outstanding TON of 17 300 was achieved using 25 ppm of this NHC–Mn(I) complex in the reduction of acetophenone.[13i] As a key observation, the reaction efficiency was found to be strongly dependent on temperature especially for low catalyst loadings where higher temperatures resulted in faster catalyst deactivation.

Up until now, several challenges remain to be confronted before earth-abundant transition metal catalytic systems can be practically utilized in (industrial) organic synthesis. For example, when compared to their noble metal counterparts, catalyst loadings remain up to four orders of magnitude higher at several thousands of ppm (*i.e.* 0.1–1.0 mol%).[12] Moreover, in order to reduce operational costs, it is desirable to replace phosphine-based ligands that are a feature of precious metal catalysts for simpler and more scalable alternatives.

As part of our ongoing program, ligand design has been at the cornerstone of our efforts in developing transition metal complexes that can promote transformations such as ethylene polymerization[16] and the (de)hydrogenation of biomass-carbonyl compounds[17,18] for the production of fine chemicals and new materials. In particular, we have found the 8-amino-5,6,7,8-tetrahydroquinoline and 8-imino-5,6,7-trihydroquinoline skeletons as useful structural motifs that can be used as *NN*-chelating ligands or derivatized to expand the denticity of the coordinating ligand.[19,20] Based on this design strategy, we herein disclose five new *NN*-manganese(I) carbonyl complexes bearing either an *N*-R substituted (R = *i*-Pr, *n*-Bu, Bn, Ph) 5,6,7,8-tetrahydroquinoline-8-amine (Scheme 1c) or a *N*-NHPh-substituted 8-imino-5,6,7-trihydroquinoline; a related *NNN*-manganese(I) complex incorporating an *N*-ethyl-1*H*-benzimazole-functionalized 5,6,7,8-tetrahydroquinoline-8-amine is also reported. All six complexes are then explored initially as precatalysts for the TH of acetophenone to determine their relative effectiveness before extending the most promising system to the TH of a wide range of alkyl- and aryl-containing ketones and aldehydes. Besides the in-depth catalytic evaluation, full details are presented for the synthesis of both the ligands, complexes and attempts to characterize intermediates involved in the catalysis.

Results and discussion

Synthesis and characterization of manganese(I) complexes (Mn1–Mn6)

Treatment of $Mn(CO)_5Br$ with *N*-R-8-N(H)$C_9H_{10}N$ (R = *i*-Pr **L1**, *n*-Bu **L2**, Bn **L3**, Ph **L4**) or imine-containing 8-(PhHN-N)C_9H_9N (**L5**) in tetrahydrofuran at 60 °C for 12 h gave on work-up, [(*NN*)$Mn(CO)_3$]Br [*NN* = **L1** (**Mn1**), **L2** (**Mn2**), **L3** (**Mn3**), **L4** (**Mn4**), **L5** (**Mn5**)], in good yield (Scheme 2). On the other hand, the preparation of the *N*-ethyl-1*H*-benzimazole-functionalized [(*NNN*)$Mn(CO)_2$]Br (**Mn6**) required more forcing conditions involving the reaction of *N*-((CH$_2$)$_2$CHN$_2$HC$_6$H$_4$)-8-N(H)$C_9H_{10}N$ (**L6**) with $Mn(CO)_5Br$ in toluene at 110 °C for 24 h. The ligands themselves, **L1–L6**, were synthesized in good overall yield *via* the interaction of 5,6,7-trihydroquinolin-8-one[7b] with the corresponding amine under reductive amination (**L1–L4**, **L6**) or condensation (**L5**) conditions (see ESI†).[18,19] All six manganese complexes were found to be stable under atmospheric conditions in the solid state but slowly decomposed under exposure to light. Complex characterization was achieved using $^1H/^{13}C$ NMR, FT-IR spectroscopy and elemental analysis (Fig. S1–S18, see ESI†).

In the ^{13}C NMR spectra of **Mn1–Mn6**, the metal-carbonyls were seen as three low intensity downfield signals in the range δ 218–223 ppm.[13–15,18] By contrast, three strong absorption peaks for the CO groups were visible between 1904 to 2027 cm^{-1} in their IR spectra (Table 1). Notably the average carbonyl stretching frequencies for **Mn1–Mn4** follow the order **Mn4** (1960) > **Mn3** (1953) > **Mn2** (1950) > **Mn1** (1948), which support the donating properties of the *N*-R substituent being:

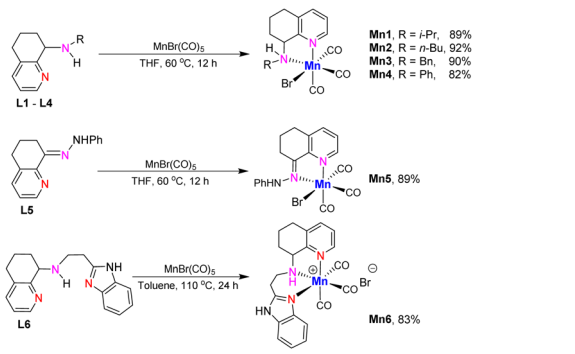

Scheme 2 Synthetic routes to manganese(I) complexes, **Mn1–Mn6**.

Table 1 ^{13}C NMR and IR spectroscopic data for the manganese complexes **Mn1–Mn6**

Complex	Chemical shift of the Mn-COs[a] (ppm)	CO stretching frequencies[b] (cm^{-1})
Mn1	222.2, 222.8, 223.0	1906, 1922, 2017
Mn2	222.0, 222.5, 223.1	1901, 1926, 2023
Mn3	220.0, 220.8, 222.4	1904, 1936, 2019
Mn4	220.8, 222.6, 223.2	1907, 1949, 2023
Mn5	219.0, 221.3, 223.3	1919, 1942, 2027
Mn6	218.9, 219.8, 220.2	1912, 1930, 2027

[a] ^{13}C NMR spectra were recorded in DMSO-d_6. [b] FT-IR spectra have been recorded in the solid state.

i-Pr > *n*-Bu > Bn > Ph. The elemental analyses of all six complexes were in support of the proposed compositions.

Crystals of **Mn1** as well as the bromide salt of **L1**, [**L1**H]Br, suitable for single crystal X-ray determinations were grown by the slow diffusion of hexane into a dichloromethane solution of the corresponding compound. ORTEP views of the resulting structures are shown in Fig. 1, while selected bond distances and angles for **Mn1** are given in the caption. Inspection of the structure of **Mn1** reveals the manganese center to be surrounded by an *NN*-chelating **L1**, three carbonyl ligands and a terminal bromide so as to complete a distorted octahedral coordination geometry. The CO ligands are disposed in a *fac* arrangement with the two nitrogen donors belonging to **L1** and bromide occupying the *trans* sites. Some variation in the Mn–N distances was evident with that involving the tetrahydroquinoline nitrogen slightly shorter than that for the amine nitrogen [Mn–N1 2.046(2) Å *vs.* Mn–N2 2.116(2) Å] in line with the better donor properties of the former. Similar observations have been noted with structurally related *NNN*- and *NNS*-manganese complexes (see **Mn7** and **Mn10**, Fig. 2),[18] though the variation was less distinct. Within the carbocyclic section of the tetrahydroquinoline, some puckering of the ring is observed on account of the sp^3-hybridized carbons, C5, C6, C5 and C8. In turn this leads to some deviation of the N–C–C–N coordination plane from planarity [N1–C9–C8–N2 torsion = −30.8°]. There were no intermolecular contacts of note.

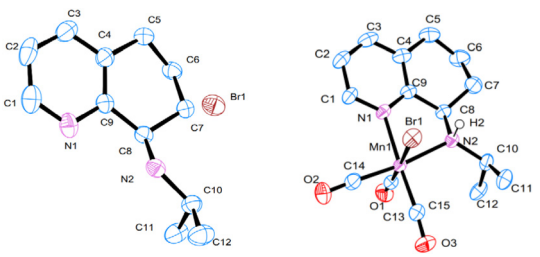

Fig. 1 ORTEP representations of [**L1**H]Br (left) and **Mn1** (right) with the thermal ellipsoids shown at the 30% probability level; the hydrogen atoms have been omitted for clarity. Selected bond distances (Å) for **Mn1**: Br1–Mn1 2.5275(4), Mn1–N1 2.046(2), Mn–N2 2.116(2); Selected bond angles (°) for **Mn-1**: N1–Mn1–Br 86.42(6), N1–Mn1–N2 78.74(8), C13–Mn1–Br1 178.75(8), C13–Mn1–N1 92.79(10), C13–Mn1–C14 90.76 (12), C13–Mn1–N2 95.38(10), N2–Mn1–Br1 85.43(6).

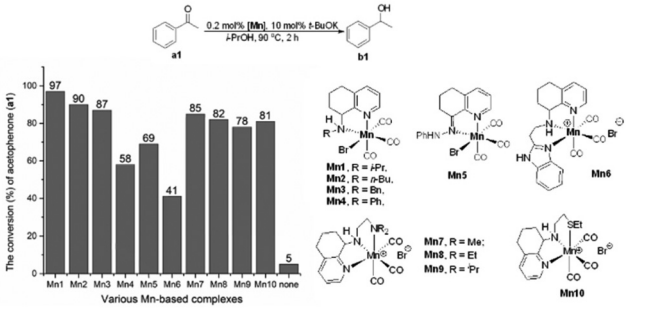

Fig. 2 Evaluation of **Mn1–Mn10** as catalysts for transfer hydrogenation of acetophenone (**a1**). Conditions: 5.0 mmol **a1**, 10 μmol (0.2 mol%) [**Mn**], 0.5 mmol *t*-BuOK (10 mol%), 5 mL *i*-PrOH, 90 °C (oil bath temperature), 2 h. The conversions were determined by GC with dodecane as the internal standard.

Catalytic studies

Optimization of the catalytic protocol. With a view to exploring the relative ability of **Mn1–Mn6** to promote the transfer hydrogenation of ketones, acetophenone (**a1**) was employed as the benchmark substrate, *t*-BuOK as the base and 2-propanol as the source of hydrogen (Fig. 2). To complement this study, the previously reported *NNN*- and *NNS*-manganese complexes, [(8-(2-YCH$_2$CH$_2$)NHC$_9$H$_{10}$N)Mn(CO)$_3$]Br (Y = NMe$_2$ **Mn7**, NEt$_2$ **Mn8**, N^{i}Pr$_2$ **Mn9**, SEt **Mn10**) (Fig. 2), that have shown effectiveness in acceptorless dehydrogenative coupling, were additionally screened.[18] Typically, these reactions were conducted in 5 mL of *i*-PrOH at 90 °C with the millimole ratio of **a1** : [**Mn**] : *t*-BuOK set at 5 : 0.01 : 0.5; the % conversions to 1-phenylethanol (**b1**) over 2 h are collected in Fig. 2.

Pleasingly, all ten manganese complexes, under these conditions stipulated, proved to be active catalysts for the reduction of **a1** with conversions to **b1** in the range of 41% to 97%. With respect to the *NN*-chelated manganese complexes **Mn1–Mn5**, the relative level of catalytic performance fell in the order: **Mn1** > **Mn2** > **Mn3** > **Mn5** > **Mn4**. Evidently, the nature of the *N*-R substituent has some effect on the catalytic performance with *i*-Pr-containing **Mn1** the most productive; imine-containing **Mn5** was notably at the lower end of the conversion range (69% conversion). The reason behind the enhanced performance for **Mn1** is uncertain but may be due to the *N*-i-Pr group providing the most suitable steric protection to inhibit deactivation pathways at high temperature.[13i] By comparison, the *N*-Ph-containing **Mn4** showed much lower conversions (58%) than seen with **Mn1–Mn3** and **Mn5**. This finding could plausibly be due to the rigidity of the *N*-Ph group leading to a barrier in the formation of active Mn–H species.[13c,d] Nevertheless, electronic factors are also likely influential and indeed the order of activity for **Mn1–Mn4** matches the trend in electron donating capacity of the *N*-R substituents seen in the IR data (*vide supra*). On the other hand, *NNN*-chelated **Mn6** incorporating the *N*-ethyl-1*H*-benzimidazole unit displayed the lowest conversion (41%) among this series of complexes. This observation can plausibly be accredited to the difficulty in the dissociation of either the

benzimidazole-nitrogen donor or a carbon monoxide ligand from the metal center to generate a vacant coordination site to allow the formation of the active Mn–H species; this observation is in accordance with that mentioned in Kundu's report.[13d] By contrast, the *NNN*- and *NNS*-type ligands in **Mn7**–**Mn10** were less influential on the conversion (range: 78% to 85%), with their relative performance being: **Mn7** > **Mn8** > **Mn10** > **Mn9**.

Overall, these results suggest that the *NN*-chelated **Mn1** is the most effective TH catalyst of this series of complexes outperforming its *NN*-counterparts as well as its *NNN* or *NNS* derivatives. As a control, we also tested the reaction in the absence of any manganese complex with the conditions otherwise identical. Significantly, only trace conversion to **b1** was observed highlighting the importance of the 3d metal complex in the TH process. Therefore, on the basis of the superior performance characteristics of **Mn1**, this complex was employed for all further studies.

With the aim to optimize the catalyst system, a selection of different bases, namely *t*-BuOK, *t*-BuONa, *i*-PrONa, EtONa, MeONa, $NaBHEt_3$, KHMDS (potassium bis(trimethylsilyl) amide), NaHMDS (sodium bis(trimethylsilyl)amide), Cs_2CO_3, Na_2CO_3, $LiOH{\cdot}H_2O$, NaOH, KOH, $Ca(OH)_2$ and $Ba(OH)_2$, was assessed with the loading of **Mn1** fixed at 0.2 mol% and base at 10 mol% (conditions *A*, Chart 1 and Table S3†). Of these fifteen bases screened, *t*-BuONa proved the most compatible allowing the greatest conversion of **a1** to **b1** of 99%. Nonetheless, more than half of the bases used displayed good performance characteristics for the TH of **a1** with conversions in the range of 86–97%. Furthermore, it was evident that the bases used in which sodium provided the counter ion were more efficient than their potassium counterparts: *t*-BuONa (99%) *vs.* *t*-BuOK (97%), NaHMDS (91%) *vs.* KHMDS (86%) and NaOH (94%) *vs.* KOH (91%) (Chart 1 and Table S3†).

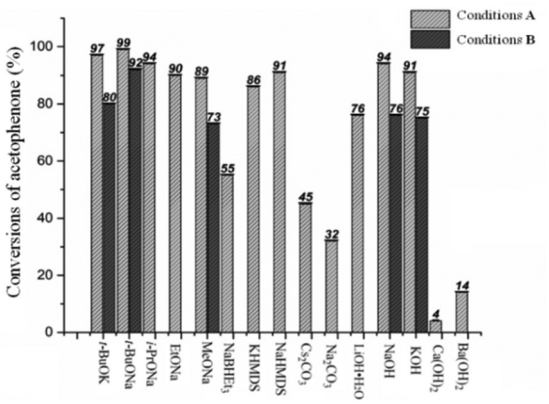

Chart 1 Transfer hydrogenation of acetophenone (**a1**) as a function of the base. Conditions *A*: 5.0 mmol **a1**, 10 μmol (0.2 mol%) **Mn1**, 0.5 mmol base (10 mol%), 5 mL *i*-PrOH, 90 °C (oil bath temperature), 2 h; Conditions *B*: 25 mmol **a1**, 5 μmol (0.02 mol%) **Mn1**, 1.25 mol base (5 mol%), 10 mL *i*-PrOH (2.5 M), 90 °C (oil bath temperature), 6 h. Notes: the conversions (%) were determined by GC with dodecane as the internal standard.

Similar findings have been reported elsewhere.[19b] Control experiments performed in the absence of either base or **Mn1** provided only trace amounts of product after 2 h at 90 °C (entries 16 and 17, Table S3†). Similarly, use of $MnBr(CO)_5$ in place of **Mn1**, under the same reaction conditions, allowed a conversion of only 6% (entry 18, Table S3†).

Next, we set about exploring the effect of varying the loading of *t*-BuONa on the TH of **a1** (Table S4†). As the base

Table 2 Screening of catalyst loading[a]

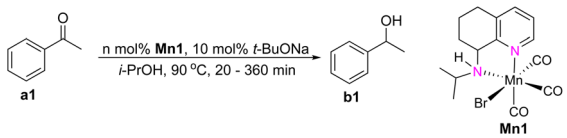

Entry	**Mn1** [*n* mol%, (*x* ppm)]	*t* (min)	Conv.[b] (%)	TON	TOF (h^{-1})
1	1.0	20	99 (92)	99	294
2	0.50	20	99	198	594
3	0.20	120	99	495	247
4	0.10	120	97	970	485
5	0.050 (500)	120	86	1720	860
6	0.025 (250)	120	82	3280	1640
7	0.020 (200)	120	78	3900	1950
8	0.010 (100)	120	71	7100	3550
9	0.0050 (50)	360	86	17 200	2867

[a] Conditions: 0.5–100 mmol **a1**, 5 μmol **Mn1**, 0.1 eq. (for **a1**) of *t*-BuONa (10 mol%), 5–100 mL *i*-PrOH (1 M), 90 °C (oil bath temperature), 20–360 min. [b] Determined by GC with dodecane as the internal standard, isolated yield in parentheses. Notes: TON = turnover number, TOF = Turnover frequency (mol of substrate per mol of complex per hour).

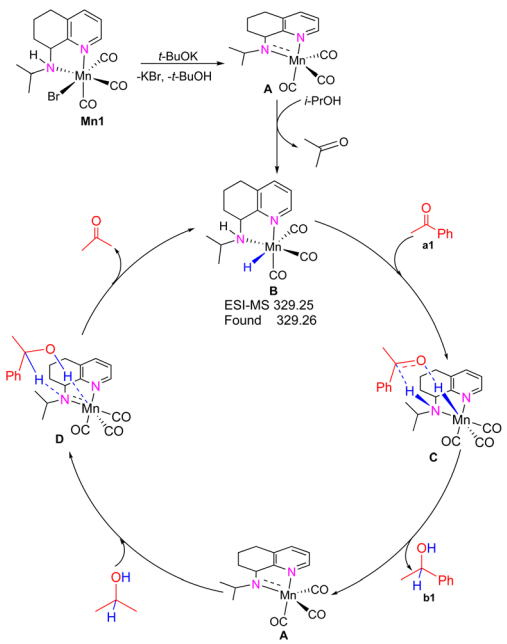

Scheme 3 One possible mechanism for the TH of **a1** promoted by **Mn1**.

loading was decreased from 25 to 1.25 mol%, a clear reduction in conversion (down to 38%) was observed. Interestingly, most cases resulted in the conversions to **b1** being over 50% with the exception of loadings of less than 2.5 mol% of *t*-BuONa. Furthermore, by prolonging the reaction time to 6 h with 5 mol% *t*-BuONa, a high conversion of 92% could be obtained (entry 9, Table S4†). On the basis of this latter finding, five selected bases, namely *t*-BuOK, *t*-BuONa, MeONa, NaOH, KOH, were additionally investigated for the reduction of **a1** with the loading set at 5 mol%, the loading of **Mn1** fixed at 0.02 mol% and the run time extended to 6 h (conditions *B*, Chart 1). Once again, *t*-BuONa proved the optimal base with the conversions of **a1** to **b1** up to 92%, while the remaining four bases also provided good conversions in the range 73 to 80%.

With the intention to explore the effect of catalyst loading on the conversion, **Mn1** was deployed at levels between 1.0 to 0.0050 mol% for the reduction of **a1** with the mol% of *t*-BuONa set at 10 mol% (Table 2). With either 1 mol% or 0.5 mol% of **Mn1** and the run temperature and duration kept at 90 °C for 20 min, respectively, essentially full conversion to **b1** was observed (entries 1 and 2, Table 2). Moreover, by extending the reaction time to 2 h, excellent conversions to **b1** could again be achieved when the catalyst loading was lowered to 0.2 or 0.1 mol%. However, further reduction of the loading from 0.050 mol% (500 ppm) to 0.010 mol% (100 ppm) saw the conversion drop from 86% to 78%, while TONs and TOFs increased up to 7100 and 3550 h^{-1}, respectively. Notably, with an exceptionally low catalyst loading of 0.0050 mol% (50 ppm), the highest TON of 17 200 was achieved with the run time extended to 360 min (6 h).

In terms of the mechanism of this TH catalysis, we propose as one possibility that **Mn1** firstly undergoes the loss of H^+ and Br^-, under the action of the base *t*-BuONa, forming amide complex **A** along with the elimination of KBr and *t*-BuOH (Scheme 3). Subsequently, the HOCH unit in *i*-PrOH adds across the Mn=N bond in **A**, to form the active hydride complex **B**. Then, the NH proton and the Mn–H hydride can

Table 3 Substrate scope for the TH of (hetero)aryl ketones[a]

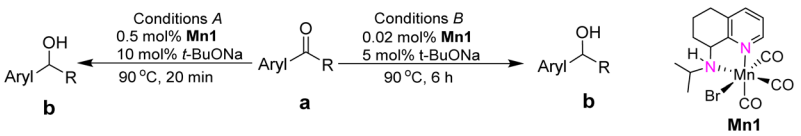

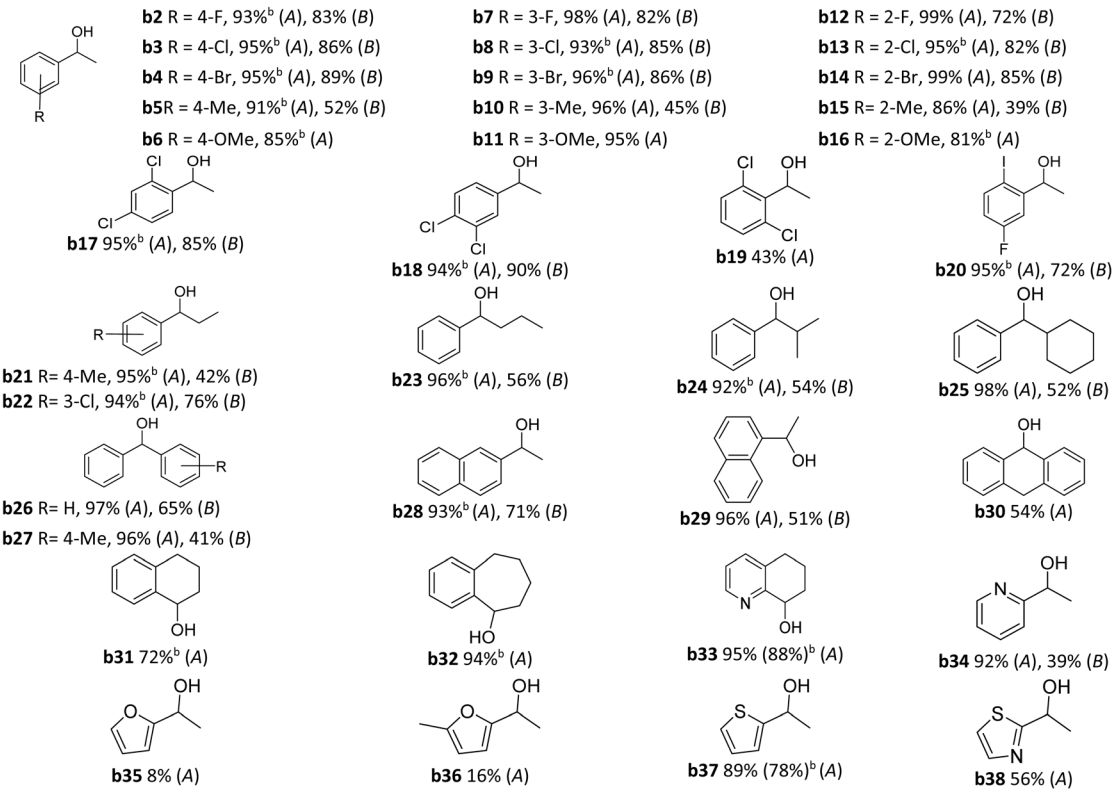

[a] Reaction conditions *A*: substrate (2.0 mmol), **Mn1** (10 μmol, 0.5 mol%), *t*-BuONa (0.2 mmol, 10 mol%), in *i*-PrOH (5 mL) at 90 °C (oil bath temperature) for 20 min. Reaction conditions *B*: substrate (25.0 mmol), **Mn1** (5 μmol, 0.02 mol%), *t*-BuONa (2.5 mmol, 10 mol%), in *i*-PrOH (25 mL) at 90 °C (oil bath temperature) for 6 h. Notes: the conversions (%) were measured using GC (*n*-dodecane was used as an internal standard). [b] Isolated % yield.

transfer by an outer-sphere pathway to **a1** (*via* transition state **C**), leading to the reduction of **a1** to **b1** and the re-formation of **A**. This proton transfer may be assisted by the conjugate acid of *t*-BuONa, which may explain its influence on conversion.[21] Finally, species **A** can dehydrogenate *i*-PrOH (*via* transition state **D**), to give acetone, thereby regenerating the active species **B**.

To lend some support for the proposed mechanism, we set about studying the process of precatalyst activation by performing a series of ^{1}H NMR experiments (Fig. S19–S21†). On the basis of these experiments, the amido complex [(*NN*)Mn(CO)$_3$] (**A** in Scheme 3) is formed when **Mn1** was treated with *t*-BuONa in the presence of *i*-PrOH at 30 °C. Indeed, related monometallic complexes have been reported as effective catalysts for the TH of ketones by Leitner[13c] and Sun.[14f] By contrast, our findings are unlike that reported in Sortais' work in which a dimeric manganese complex has been identified.[13b] Furthermore, isolated **A** displayed high activity for the TH of **a1** with good conversions (80%) observed under conditions *A*. On the other hand, treatment of **Mn1** with *t*-BuONa in the presence of *i*-PrOH at 90 °C gave what we tentatively ascribe as the active species **B** (see ESI†). Unfortunately, **B** proved very sensitive and attempts to obtain a crystal structure of this complex were unsuccessful. Nevertheless, the ESI-MS mass spectrum of **B** provided evidence for a M–H parent ion peak at *m*/*z* 329.25 [**B**–H]$^+$ (see Fig. S23†).

To gain a broader understanding of the scope of **Mn1**, we extended the TH evaluation to cover a wide variety of (hetero) aromatic ketones using two sets of conditions namely *A* (0.5 mol% **Mn1**, 10 mol% *t*-BuONa, 90 °C, 20 min) and *B* (0.02 mol% **Mn1**, 5 mol% *t*-BuONa, 90 °C, 6 h). As shown in Table 3, a wide variety of (hetero)aromatic ketones could be reduced to their corresponding alcohols. Indeed, various substituted acetophenones (**a2–a16**, Table 3) containing both electron withdrawing and donating groups on the aryl group were effectively reduced under conditions *A*. Halide-containing substrates produced the desired alcohols with conversions up to 99%. Interestingly, the acetophenone derivatives (**a2–a4**, **a7–a9**, **a12–a14**, **a17**, **a18** and **a20**) bearing electron-withdrawing substituents (R = F, Cl and Br) were more effectively converted to their corresponding alcohols (**b2–b4**, **b7–b9** and **b12–b14**) than that observed by their analogues containing electron-donating groups (**a5**, **a6**, **a10**, **a11**, **a15** and **a16**, R = Me and OMe) under conditions *B*. Evidently, these halide-containing substrates can be reduced without the formation of dehalogenated products. It was also found that acetophenones bearing *meta* or *para* substituents typically display higher conversions than those bearing *ortho* substituents (**a2–a11** *vs.* **a12–a16**, Table 3). These differences may be the result of greater steric hindrance induced by the *ortho* substituents.

With the goal to explore the effect of electronic properties and steric hindrance on catalytic performance, acetophenones containing chloride substituents (**a17–a19**) at two different positions on the aryl group were firstly investigated (Table 3). The 2,4- and 3,4-substituted derivatives **a17** and **a18** could be smoothly converted to the corresponding alcohols, **b17** and **b18**, while 2′,6′-dichloroacetophenone (**b19**) was more sluggish when compared to its analogues, **a17** and **a18**. A variety of propiophenone derivatives bearing functional groups, such as Me and Cl (**a21–a22**) were reduced to give the expected alcohols with nearly quantitative conversions (conditions *A*, Table 3). With regard to benzophenones and acetyl-naphthalenes, the conversions to the corresponding alcohols were in general high, with benzophenone, phenyl(*p*-tolyl)methanone and 1-/2-acetylnaphthalenes amenable to 97%, 96%, 93% and 96% conversion (under conditions *A*), respectively. Benzocyclones (**a30–a32**) with carbocyclic ring sizes of between six and eight gave moderate to high conversions to their corresponding alcohols, with 9,10-dihydroanthracen-9-ol, 1,2,3,4-tetrahydronaphthalen-1-ol and 6,7,8,9-tetrahydro-5*H*-benzo[7]annulen-5-ol being obtained with percentages of 54%, 72% and 94% (under conditions *A*, Table 3), respectively. When compared to 3,4-dihydronaphthalen-1(2*H*)-one (**a31**), 6,7-dihydroquinolin-8(5*H*)-one (**a33**) underwent higher conversion, with 5,6,7,8-tetra-

Table 4 Substrate scope for the TH of cyclic alkyl and acyclic dialkyl ketones[a]

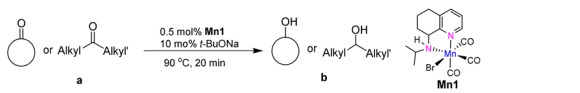

Entry	Substrate	Product	Conv.[b] (%)
1	 a39	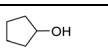 b39	69
2	 a40	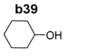 b40	94
3	 a41	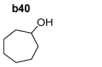 b41	90
4	 a42	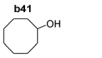 b42	84
5	 a43	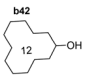 b43	72
6	 a44	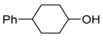 b44	90 (85)
7	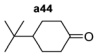 a45	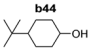 b45	81
8	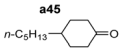 a46	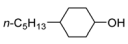 b46	91
9	 a47	 b47	60
10	 a48	 b48	65 (60)
11	 a49	 b49	99
12	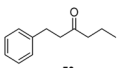 a50	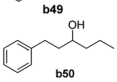 b50	93 (90)

[a] Reaction conditions *A*: substrate (2.0 mmol), **Mn1** (10 μmol, 0.5 mol%), *t*-BuONa (0.2 mmol, 10 mol%), *i*-PrOH (5 mL) at 90 °C (oil bath temperature) for 20 min. [b] Measured by GC with *n*-dodecane used as an internal standard. Isolated yields are given in parentheses.

hydroquinolin-8-ol (**b33**) being obtained in 88% isolated yield. With respect to heteroaryl ketones, **a34–a38**, the conversions to the corresponding alcohols, **b34–a38**, were slightly lower than that observed by the aryl ketones (Table 3). Notably, the 2-acetylfuran derivatives, **a35** and **a36**, gave only low conversions to their alcohols which could be due to the presence of a strongly coordinating oxygen heteroatom.

To further examine the substrate scope of **Mn1**, cyclic alkyl and acyclic dialkyl ketones were also assessed using reaction conditions *A* (Table 4). For the cyclic alkyl ketones, it was found that the ring size was influential on the conversion with the smallest ring ketone, cyclopentanone (**a39**, $n = 5$) affording the lowest conversion of 69% (entry 1, Table 4). Conversely, the medium size cyclic ketones (**a40–a42**, $6 \leq n \leq 8$) gave higher conversions, with cyclohexanol, cycloheptanol and cyclooctenone formed between 84% and 94%. On the other hand, the largest ring ketone cyclododecanone (**a43**, $n = 12$) again led to a lower conversion to alcohol **b43** (entry 5, Table 4).

With the ring size of the cyclic alkyl ketone maintained at six, the 4-substituted cyclohexan-1-ones, **a44–a47**, all gave high conversions (81–91%) to the corresponding cyclic alcohols (**b44–b47**, entries 6–8, Table 4). By contrast, 2-substituted cyclohexan-1-one, **a47**, gave a lower conversion to **b47** (60%) which likely reflects the steric properties of the 2-isopropyl substituent (entry 7, Table 4). Similarly, the N-heterocyclic containing ketone, quinuclidin-3-one **a48**, gave lower conversion (65%) to **b48** (entry 10, Table 4). By comparison, the conversions for the long chain dialkyl-containing ketones, 4-phenylbutan-2-one (**a49**) and 1-phenylhexan-3-one (**a50**), were higher at 99% and 93% in 20 min, respectively (entries 11 and 12, Table 4).

This manganese-mediated TH is not just limited to ketonic substrates. Indeed, a number of substituted aldehydes (**c1–c11**, entries 1–10, Table 5) were shown to undergo TH using reaction conditions *A*. Indeed, most of the aldehydes employed were efficiently reduced to the corresponding primary alcohol and in some cases quantitatively. The aryl-containing aldehydes, **c1–c5**, with either electron-rich or electron-poor groups gave good to high conversions to **d1** (90%), **d2** (99%), **d3** (85%), **d4** (99%) and **d5** (99%), respectively (entries 1–5, Table 5). Heteroatom-containing aldehydes, picolinaldehyde (**c6**), thiophene-2-carboxaldehyde (**c7**) and furan-2-carbaldehyde (**c8**) also worked effectively (entries 6–8, Table 5). Finally, our catalytic system also promoted the reduction of the long chain alkyl-containing aldehydes, heptaldehyde (**c9**) and octanal (**c10**) affording excellent conversions (entries 9 and 10, Table 5).

Table 5 Substrate scope for the TH of aldehydes[a]

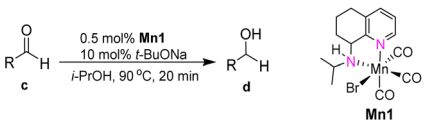

Entry	Substrate	Product	Conv.[b] (%)
1			90 (85)
2			99 (95)
3			85 (81)
4			99 (94)
5			99 (95)
6			46 (41)
7			98 (93)
8			89 (82)
9			99
10			99

[a] Reaction conditions *A*: aldehyde (**c**) (2.0 mmol), **Mn1** (10 umol, 0.5 mol%), *t*-BuONa (0.2 mmol, 10 mol%), *i*-PrOH (5 mL) at 90 °C (oil bath temperature) for 30 min. [b] Measured by GC with *n*-dodecane used as an internal standard. Isolated yields are given in parentheses.

Conclusions

In summary, a new set of *NN*-manganese carbonyl complexes (**Mn1–Mn5**) along with the *NNN*-containing **Mn6**, all incorporating either an 8-amino-5,6,7,8-tetrahydroquinoline or an 8-imino-5,6,7-trihydroquinoline backbone, have been synthesized and characterized. All six complexes, along with previously reported *NNN*- and *NNS*-complexes, **Mn7–Mn10** (Fig. 2), have been evaluated as catalysts for the transfer hydrogenation of acetophenone. Notably, isopropyl containing *NN*-**Mn1**, in the presence of *t*-BuONa, proved the most effective and was able to operate efficiently with a catalyst loading of just 0.005 mol%. Indeed, using **Mn1**/*t*-BuONa as catalyst, a wide range of (hetero)aromatic-, aliphatic- and cycloalkyl-containing ketones (50 examples) and aldehydes (10 examples) could be reduced to give their corresponding alcohols with conversions in the range 39–99%. Furthermore, the catalytic results suggest an outer-sphere hydrogen transfer involving the amino NH functionality in **Mn1** as the proton source. Further mechanistic studies are currently ongoing to elucidate the detailed catalytic cycle.

Experimental section

General information

All manipulations were carried out under a nitrogen atmosphere using standard Schlenk techniques. All solvents were dried and distilled under nitrogen prior to use. All substrates,

both liquid and solid, were used directly without further purification. Other reagents were purchased from Aldrich, Acros or local suppliers. ^{1}H and ^{13}C NMR spectra were recorded on Bruker AV-400 NMR and Bruker AV-500 NMR spectrometers. Chemical shift values in the ^{1}H and ^{13}C NMR spectra were referenced internally to the residual solvent resonances. Infrared spectroscopy was performed in the solid state on a Bruker ALPHA. Elemental analysis was performed with a Vario EL III CHN microanalyzer. GC was performed using a FuLi GC-9790Plus instrument (Zhe Jiang FuLi Analytical Instrument) using a PB-FFAP column (30 m × 0.32 mm × 0.25 μm, Wuhan Puli Technology Co., Ltd) or RB-WAX column (30 m × 0.25 mm × 0.25 μm, Wuhan Puli Technology Co., Ltd): injector temp. 300 °C, detector temp. 300 °C, column temp. 120 °C, withdraw time 2 min, then 20 °C min^{-1} to 180 °C for 5 min, then 20 °C min^{-1} to 250 °C, withdraw time for 5 min. Synthetic procedures for **L1–L6** and **Mn1–Mn6** are given in the ESI†.

Transfer hydrogenation studies

Under an atmosphere of nitrogen, a 25–250 mL dried Schlenk tube, containing a stirrer bar, was charged with the selected ketonic substrate (2.5–25.0 mmol), manganese complex (**Mn1–Mn10**, 5.0–10.0 μmol), the desired amount of base (*e.g.* *t*-BuOK, *t*-BuONa, *i*-PrONa, NaOEt, NaOMe KOH, NaOH, $CsCO_3$, Na_2CO_3, $LiOH{\cdot}H_2O$, LiOH, $Ca(OH)_2$, K_2CO_3, Na_2CO_3, $NaBHEt_3$, NaHMDS, KHMDS) (0.5–4.0 mmol) and *i*-PrOH (5–100 mL). The vessel was sealed and the contents then stirred at 90 °C (oil bath temperature). After the desired reaction time, the mixture was allowed to cool to room temperature and the pressure slowly released. The reaction mixture was filtered through a plug of silica gel and then analyzed by GC; the composition of the reaction mixture was confirmed by running a separate GC on a mixture of pure ketone, alcohol and dodecane. All conversions were determined by GC using dodecane as internal standard. Where indicated, the crude products were purified by flash gel chromatography (eluent: petroleum ether/ethyl acetate = 200 : 1 to 10 : 1) and an isolated yield determined.

X-ray structure determination

The single-crystal X-ray diffraction studies of [**L1**H]Br and **Mn1** were conducted on a Rigaku Sealed Tube CCD (Saturn 724+) diffractometer with graphite-mono chromated Cu-Kα radiation (λ = 1.54184) at 169(8) K and the cell parameters obtained by global refinement of the positions of all collected reflections. Intensities were corrected for Lorentz and polarization effects and empirical absorption. The structures were solved by direct methods and refined by full-matrix least-squares on F^2. All non-hydrogen atoms were refined anisotropically and all hydrogen atoms were placed in calculated positions. Structure solution was performed using SHELXL (2015) and structure refinement performed using SHELXL.[22] Crystal data and processing parameters for [**L1**H]Br and **Mn1** are summarized in Table S6.†

Conflicts of interest

Acknowledgements

We acknowledge the support from the Nature Science Foundation of Hebei Province (B2022205020, B2022204020) and Talent Introduction Foundation of Hebei Agricultural University (YJ201931). Research Project of Fundamental Scientific Research Business Expenses of Provincial Colleges and Universities in Hebei Province (KY2021028); Opening Fund of CAS Key Laboratory of Engineering Plastics, Institute of Chemistry. G.A.S. is grateful to the Chinese Academy of Sciences for a President's International Fellowship for Visiting Scientists.

References

1 (*a*) P. G. Andersson and I. J. Munslo, in *Modern Reduction Methods*, Wiley, New York, 2008; (*b*) P. A. Dub and T. Ikariya, *ACS Catal.*, 2012, **2**, 1718–1741; (*c*) J. Ito and H. Nishiyama, *Tetrahedron Lett.*, 2014, **55**, 3133–3146; (*d*) D. Wang and D. Astruc, *Chem. Rev.*, 2015, **115**, 6621–6686; (*e*) L. Shi, Y. Liu, Q. Liu, B. Wei and G. Zhang, *Green Chem.*, 2012, **14**, 1372–1375.

2 (*a*) E. J. Corey, R. K. Bakshi and S. Shibata, *J. Am. Chem. Soc.*, 1987, **109**, 5551–5553; (*b*) L. Deloux and M. Srebnik, *Chem. Rev.*, 2002, **93**, 763–784; (*c*) D. Lunic, N. Sanosa, I. Funes-Ardoiz and C. J. Teskey, *Angew. Chem., Int. Ed.*, 2022, **61**, e202207647.

3 (*a*) A. Matsunami and Y. Kayaki, *Tetrahedron Lett.*, 2018, **59**, 504–513; (*b*) D. Baidilov, D. Hayrapetyan and A. Y. Khalimon, *Tetrahedron*, 2021, **98**, 132435.

4 Selected examples for TH ruthenium catalysts, see. (*a*) A. Fujii, S. Hashiguchi, N. Uematsu, T. Ikariya and R. Noyori, *J. Am. Chem. Soc.*, 1996, **118**, 2521–2522; (*b*) A. Del Zotto, W. Baratta, M. Ballico, E. Herdtweck and P. Rigo, *Organometallics*, 2007, **26**, 5636–5642; (*c*) W. Baratta, G. Chelucci, S. Magnolia, K. Siega and P. Rigo, *Chem. – Eur. J.*, 2009, **15**, 726–732; (*d*) W. Du, P. Wu, Q. Wang and Z. Yu, *Organometallics*, 2013, **32**, 3083–3090; (*e*) H. Chai, T. Liu, Q. Wang and Z. Yu, *Organometallics*, 2015, **34**, 5278–5284; (*f*) J. M. Botubol-Ares, S. Cordón-Ouahhabi, Z. Moutaoukil, I. G. Collado, M. Jiménez-Tenorio, M. C. Puerta and P. Valerga, *Organometallics*, 2021, **40**, 792–803; (*g*) A. Dubey and E. Khaskin, *ACS Catal.*, 2016, **6**, 3998–4002.

5 (*a*) K. Murata, T. Ikariya and R. Noyori, *J. Org. Chem.*, 1999, **64**, 2186–2187; (*b*) K. Farrell, H. Müller-Bunz and M. Albrecht, *Organometallics*, 2015, **34**, 5723–5733.

6 Selected examples for TH iridium catalysts, see. (*a*) M. Albrecht, J. R. Miecznikowski, A. Samuel, J. W. Faller and R. H. Crabtree, *Organometallics*, 2002, **21**, 3596–3604; (*b*) U. Hintermair, J. Campos, T. P. Brewster, L. M. Pratt, N. D. Schley and R. H. Crabtree, *ACS Catal.*, 2014, **4**, 99–

108; (*c*) R. Wang, X. Han, J. Xu, P. Liu and F. Li, *J. Org. Chem.*, 2020, **85**, 2242–2249.

7 Selected examples for TH osmium catalysts, see. (*a*) W. Baratta, M. Ballico, G. Chelucci, K. Siega and P. Rigo, *Angew. Chem., Int. Ed.*, 2008, **47**, 4362–4365; (*b*) W. Baratta, F. Benedetti, A. Del Zotto, L. Fanfoni, F. Felluga, S. Magnolia, E. Putignano and P. Rigo, *Organometallics*, 2010, **29**, 35639; (*c*) G. Chelucci, S. Baldino and W. Baratta, *Acc. Chem. Res.*, 2015, **48**, 363–379; (*d*) J. P. C. Coverdale, I. Romero-Canelón, C. Sanchez-Cano, G. J. Clarkson, A. Habtemariam, M. Wills and P. J. Sadler, *Nat. Chem.*, 2018, **10**, 347–354.

8 T. Zell and R. Langer, *ChemCatChem*, 2018, **10**, 1930–1940.

9 F. Kallmeier and R. Kempe, *Angew. Chem., Int. Ed.*, 2018, **57**, 46–60.

10 (*a*) T. Zell and D. Milstein, *Acc. Chem. Res.*, 2015, **48**, 1979–1994; (*b*) Y.-Y. Li, S.-L. Yu, W.-Y. Shen and J.-X. Gao, *Acc. Chem. Res.*, 2015, **48**, 2587–2598; (*c*) D. Wei and C. Darcel, *Chem. Rev.*, 2019, **119**, 2550–2610; (*d*) P. O. Lagaditis, A. J. Lough and R. H. Morris, *J. Am. Chem. Soc.*, 2011, **133**, 9662–9665; (*e*) R. Bigler, R. Huber and A. Mezzetti, *Angew. Chem., Int. Ed.*, 2015, **54**, 5171–5174; (*f*) R. A. Farrar–Tobar, B. Wozniak, A. Savini, S. Hinze, S. Tin and J. G. de Vries, *Angew. Chem., Int. Ed.*, 2019, **58**, 1129–1133; (*g*) X. Liu, J. G. de Vries and T. Werner, *Green Chem.*, 2019, **21**, 5248–5255; (*h*) S. Zhang, Z. Wang, Q. Cao, E. Yue, Q. Liu, Y. Ma, T. Liang and W.-H. Sun, *Dalton Trans.*, 2020, **49**, 15821–15827.

11 (*a*) W. Liu, B. Sahoo, K. Junge and M. Beller, *Acc. Chem. Res.*, 2018, **51**, 1858–1869; (*b*) A. Mukherjee and D. Milstein, *ACS Catal.*, 2018, **8**, 11435–11469; (*c*) W. Ai, R. Zhong, X. Liu and Q. Liu, *Chem. Rev.*, 2018, **119**, 2876–2953; (*d*) G. Zhang and S. K. Hanson, *Chem. Commun.*, 2013, **49**, 10151–10153; (*e*) C. Hou, J. Jiang, Y. Li, Z. Zhang, C. Zhao and Z. Ke, *Dalton Trans.*, 2015, **44**, 16573–16585.

12 (*a*) E. S. Gulyaeva, E. S. Osipova, R. Buhaibeh, Y. Canac, J.-B. Sortais and D. A. Valyaev, *Coord. Chem. Rev.*, 2022, **458**, 214421; (*b*) K. Azouzi, D. A. Valyaev, S. Bastin and J.-B. Sortais, *Curr. Opin. Green Sustainable Chem.*, 2021, **31**, 100511; (*c*) K. Das, S. Waiba, A. Jana and B. Maji, *Chem. Soc. Rev.*, 2022, **51**, 4386–4464; (*d*) Y. Wang, M. Wang, Y. Li and Q. Liu, *Chem*, 2021, **7**, 1180–1223.

13 (*a*) M. Perez, S. Elangovan, A. Spannenberg, K. Junge and M. Beller, *ChemSusChem*, 2017, **10**, 83–86; (*b*) A. Bruneau-Voisine, D. Wang, V. Dorcet, T. Roisnel, C. Darcel and J.-B. Sortais, *Org. Lett.*, 2017, **19**, 3656–3659; (*c*) O. Martínez-Ferraté, C. Werlé, G. Franciò and W. Leitner, *ChemCatChem*, 2018, **10**, 4514–4518; (*d*) K. Ganguli, S. Shee, D. Panja and S. Kundu, *Dalton Trans.*, 2019, **48**, 7358–7366; (*e*) A. Dubey, S. M. W. Rahaman, R. R. Fayzullin and J. R. Khusnutdinova, *ChemCatChem*, 2019, **11**, 3844–3852; (*f*) C. Zhang, B. Hu, D. Chen and H. Xia, *Organometallics*, 2019, **38**, 3218–3226; (*g*) V. Vigneswaran, S. N. MacMillan and D. C. Lacy, *Organometallics*, 2019, **38**, 4387–4391; (*h*) N. V. Shvydkiy, O. Vyhivskyi, Y. V. Nelyubina and D. S. Perekalin, *ChemCatChem*, 2019, **11**, 1602–1605; (*i*) R. Putten, J. Benschop, V. J. Munck, M. Weber, C. Müller, G. A. Filonenko and E. A. Pidko, *ChemCatChem*, 2019, **11**, 5232–5235; (*j*) D. Wang, A. Bruneau-Voisine and J.-B. Sortais, *Catal. Commun.*, 2018, **105**, 31–36; (*k*) S. Budweg, K. Junge and M. Beller, *Chem. Commun.*, 2019, **55**, 14143–14146.

14 Selected examples for ATH manganese catalysts:. (*a*) A. Zirakzadeh, S. R. M. M. Aguiar, B. Stöger, M. Widhalm and K. Kirchner, *ChemCatChem*, 2017, **9**, 1744–1748; (*b*) D. Wang, A. Bruneau-Voisine and J.-B. Sortais, *Catal. Commun.*, 2018, **105**, 31–36; (*c*) R. van Putten, G. A. Filonenko, A. Gonzalez de Castro, C. Liu, M. Weber, C. Müller, L. Lefort and E. Pidko, *Organometallics*, 2019, **38**, 3187–3196; (*d*) G.-Y. Zhang, S.-H. Ruan, Y.-Y. Li and J.-X. Gao, *Chin. Chem. Lett.*, 2021, **32**, 1415–1418; (*e*) K. Azouzi, A. Bruneau-Voisine, L. Vendier, J.-B. Sortais and S. Bastin, *Catal. Commun.*, 2020, **142**, 106040; (*f*) L. Wang, J. Lin, Q. Sun, C. Xia and W. Sun, *ACS Catal.*, 2021, **11**, 8033–8041; (*g*) J. Yang, L. Yao, Z. Wang, Z. Zuo, S. Liu, P. Gao, M. Han, Q. Liu, G. A. Solan and W.-H. Sun, *J. Catal.*, 2023, **418**, 40–50; (*h*) K. Z. Demmans, M. E. Olson and R. H. Morris, *Organometallics*, 2018, **37**, 4608–4618; (*i*) H. Jayaprakash, *Dalton Trans.*, 2021, **50**, 14115–14119; (*j*) H. Jayaprakash, P. Coburger, M. Worle, A. Togni and H. Grutzmacher, *Chem. – Eur. J.*, 2022, **28**, e202201522; (*k*) F. Li, L. Long, Y. M. He, Z. Li, H. Chen and Q. H. Fan, *Angew. Chem., Int. Ed.*, 2022, **61**, e202202972; (*l*) C. L. Oates, A. S. Goodfellow, M. Buhl and M. L. Clarke, *Angew. Chem., Int. Ed.*, 2023, **62**, e202212479.

15 (*a*) J. A. Garduño, M. Flores–Alamo and J. J. García, *ChemCatChem*, 2019, **11**, 5330–5338; (*b*) D. Wei, A. Bruneau–Voisine, M. Dubois, S. Bastin and J. B. Sortais, *ChemCatChem*, 2019, **11**, 5256–5259; (*c*) C. L. Oates, M. B. Widegren and M. L. Clarke, *Chem. Commun.*, 2020, **56**, 8635–8638; (*d*) X. Liu and T. Werner, *Chem. Sci.*, 2021, **12**, 10590–10597; (*e*) K. Sarkar, K. Das, A. Kundu, D. Adhikari and B. Maji, *ACS Catal.*, 2021, **11**, 2786–2794.

16 (*a*) Z. Wang, Q. Liu, G. A. Solan and W.-H. Sun, *Coord. Chem. Rev.*, 2017, **350**, 68–83; (*b*) Z. Wang, G. A. Solan, W. Zhang and W.-H. Sun, *Coord. Chem. Rev.*, 2018, **363**, 92–108; (*c*) Q. Mahmood, X. Li, L. Qin, L. Wang and W.-H. Sun, *Dalton Trans.*, 2022, **51**, 14375–14407.

17 (*a*) B. Pan, B. Liu, E. Yue, Q. Liu, X. Yang, Z. Wang and W.-H. Sun, *ACS Catal.*, 2016, **6**, 1247–1253; (*b*) Z. Wang, X. Chen, B. Liu, Q. Liu, G. A. Solan, X. Yang and W.-H. Sun, *Catal. Sci. Technol.*, 2017, **7**, 1297–1304; (*c*) Z. Wang, B. Pan, Q. Liu, E. Yue, G. A. Solan, Y. Ma and W.-H. Sun, *Catal. Sci. Technol.*, 2017, **7**, 1654–1661; (*d*) Z. Wang, Y. Li, Q. Liu, G. A. Solan, Y. Ma and W.-H. Sun, *ChemCatChem*, 2017, **9**, 4275–4281.

18 Z. Wang, Q. Lin, N. Ma, S. Liu, M. Han, X. Yan, Q. Liu, G. A. Solan and W.-H. Sun, *Catal. Sci. Technol.*, 2021, **11**, 8026–8036.

19 (*a*) J. Li, Y. Ma, Z. Wang, Q. Liu, G. A. Solan, Y. Ma and W.-H. Sun, *Dalton Trans.*, 2018, **47**, 8738–8745; (*b*) Z. Wang, Y. Liu, M. Han, N. Ma, Q. Lyu, Q. Liu and W.-H. Sun, *Dalton Trans.*, 2022, **51**, 10983–10991; (*c*) F. Cao, Y. Wang, X. Wang, W. Zhang, G. A. Solan, R. Wang, Y. Ma, X. Hao and W.-H. Sun, *Catal. Sci. Technol.*, 2022, **12**, 6687–6703.

20 (*a*) D. Zerla, G. Facchetti, M. Fusè, M. Pellizzoni, C. Castellano, E. Cesarotti, R. Gandolfi and I. Rimoldi, *Tetrahedron: Asymmetry*, 2014, **25**, 1031–1037; (*b*) D. S. Zerla, I. Rimoldi, E. Cesarotti, G. Facchetti, M. Pellizzoni and M. Fusè, *J. Organomet. Chem.*, 2014, **771**, 2–8.

21 (*a*) R. van Putten, E. A. Uslamin, M. Garbe, C. Liu, A. Gonzalez-de-Castro, M. Lutz, K. Junge, E. J. M. Hensen, M. Beller, L. Lefort and E. A. Pidko, *Angew. Chem., Int. Ed.*, 2017, **56**, 7531–7534; (*b*) Y. Wang, S. Liu, H. Yang, H. Li, Y. Lan and Q. Liu, *Nat. Chem.*, 2022, **14**, 1233–1241.

22 (*a*) G. M. Sheldrick, *Acta Crystallogr., Sect. A: Found. Adv.*, 2015, **A71**, 3–8; (*b*) G. M. Sheldrick, *Acta Crystallogr., Sect. C: Struct. Chem.*, 2015, **C71**, 3–8.